Gas-Phase Experimental and Theoretical Near Edge X-ray Absorption Fine Structure Study of 2-Mercaptobenzothiazole

G. Contini,*,† V. Carravetta,‡ V. Di Castro,§ S. Stranges,§ R. Richter,|| and M. Alagia⊥

CNR, Institute of Mineral Processing, Via Bolognola 7, 00138 Rome, Italy, ICQEM-CNR, Via Alfieri 1, Ghezzano, I-56010 San Giuliano Terme (PI), Italy, Dipartimento di Chimica, Università di Roma "La Sapienza" ed Unità INFM, P. le A. Moro 5, 00185 Rome, Italy, Sincrotrone Trieste, 34012 Basovizza, Trieste, Italy, and TASC-INFM, Area Science Park, Basovizza, 34012 Trieste

Received: March 7, 2001; In Final Form: May 4, 2001

Near edge X-ray absorption fine structure (NEXAFS) spectra of 2-mercaptobenzothiazole have been investigated from experimental and theoretical points of view. High-resolution NEXAFS spectra (total-ion-yield) have been obtained in the gas phase near the carbon and nitrogen K-edges, and sulfur $L_{2,3}$-edges using synchrotron radiation. The experimental data are interpreted with the help of static-exchange (STEX) ab initio calculations for the different edges and compared with previously reported experimental and theoretical spectra of a similar molecule, the 2-mercaptobenzoxazole. The good agreement between experiment and theory allows for a detailed discussion and assignment of the various features observed. A vibrational progression at the C K-edge is also identified in the highly resolved experimental spectrum.

I. Introduction

The study of heterocyclic molecules with aromatic rings and their adsorption on metals is of considerable importance from both a theoretical and a technological point of view. These molecules are interesting because of their applications as corrosion inhibitors and flotation collectors and for their ability to form self-assembled layers. In this respect, NEXAFS spectroscopy of molecules free and interacting with surfaces provides a well-established tool in chemical physics.[1] Molecules that are solids at room temperature and pressure, like 2-mercaptobenzothiazole ($C_7H_5NS_2$, in the following MBT), can be vaporized in a vacuum onto a surface to form adsorbed layers. It is crucially important to study the species in the vapor phase, this being the entity interacting with the surrounding environment in the condensed phase.

In this paper we report the first NEXAFS spectra (total-ion-yield) at the C K-, N K-, and S L-edges obtained experimentally for MBT in the gas phase at high resolution. Ab initio theoretical photoabsorption cross sections computed with full account of core−hole effects are also presented and compared with the experimental results. The direct static exchange technique (STEX),[2] a fully ab initio method thoroughly tested in various contexts,[3] is employed here for a detailed assignment of the spectra. A recent paper[4] reported a similar experimental study on solid MBT by NEXAFS spectroscopy. That investigation, however, regarded only the spectra measured by partial electron yield at the N K- and S L-edges (in a photon range region smaller than the one considered here) and did not include the C K-edge spectrum. In section IV it will be shown that the present experimental spectra allow comparison with theory and complete interpretation in terms of electronic structure of the molecule. Vibrational resolved structures at the C K-edge are also identified.

II. Experimental Section

The experiment has been carried out using the ARPES end-station of the gas-phase beamline at Elettra. Details of the beamline and the experimental station have been given elsewhere.[5] NEXAFS spectra were obtained as total-ion-yields using a time-of-flight mass spectrometer in the direction of the light polarization vector. Mass spectra recorded at 21.22 eV photon energy showed no peaks with masses higher than the molecular one. The photon energy calibration of the two gratings used in the sulfur $L_{2,3}$-edge and carbon K-edge regions is based on the Kr $3d_{5/2} \rightarrow 6p$ and $3d_{3/2} \rightarrow 5p$ resonance lines (valley at 92.51 eV[6]), the Ar $2p_{3/2} \rightarrow 4s$ resonance feature recorded first and second diffraction order (244.37 eV[7]), the SF_6 absorption peak at 178.63 eV,[8] and the N_2 $1s \rightarrow \pi^*$ vibronic resonances (second and first order lines at 200.55 and 401.10 eV, respectively[7]). During the experiment the photon energy calibration was checked by recording total-ion-yield spectra of Ar in the $2p_{3/2} \rightarrow 4s$ excitation region and N_2 $1s \rightarrow \pi^*$ vibronic resonances in a gas cell located behind the experimental chamber using first- and second-order monochromator scans.

The NEXAFS spectra shown in the text have been obtained as a sum of several scans. The C K-edge spectrum in the 285.0−290.6 eV energy range was recorded using 30 meV resolution, 8 meV step, and 80 s/point total acquisition time; the same spectrum in the 290.6−319.0 eV energy range was recorded with 50 meV resolution, 25 s/point total acquisition time, and 50 meV step from 290.6 to 299.0 eV and 100 meV step from 299.0 to 319.0 eV. The spectra in the S L-edge and N K-edge regions were recorded with 30 and 70 meV resolution, respectively. In the N K-edge spectrum a 15 meV step and 80 s/point total acquisition time were used below 403.9 eV, while

* Corresponding author. E-mail: continig@iasi.rm.cnr.it. Fax: +39 068804463.
† CNR, Institute of Mineral Processing.
‡ ICQEM-CNR.
§ Università di Roma "La Sapienza" ed Unità INFM.
|| Sincrotrone Trieste.
⊥ TASC-INFM.

10.1021/jp010865e CCC: $20.00
Published on Web 07/06/2001

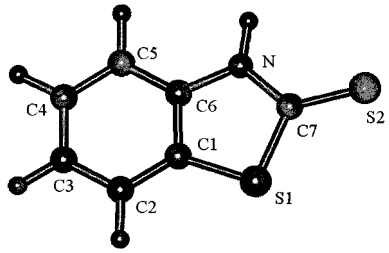

Figure 1. 2-Mercaptobenzothiazole (MBT) structure. The numbering of the seven carbon atoms is used in text.

at higher energies the conditions were 50 meV step and 40 s/point. The S L-edge spectrum reported in the upper part of Figure 7 was recorded using 7 meV step and 20 s/point acquisition time; the S L-edge spectrum reported in the lower part of Figure 7 at energies below 177.3 eV was recorded using 50 meV step and 10 s/point acquisition time, while at higher energies the conditions were 100 meV step and 5 s/point.

MBT (from Merck), purified by repeated sublimation cycles before use, was introduced into the ionization region by vaporizing the solid sample under vacuum. The temperature of the solid MBT during the measurements was kept constant at 90 °C. To minimize contamination, some elements of the spectrometer were heated and the interaction region was surrounded by a shield cooled with liquid nitrogen.

The structure of the MBT (thione form) is shown in Figure 1. MBT can exist also in the thiol tautomeric form (having the endocyclic double bond C═N and the hydrogen bonded to the sulfur atom); in the sample used in our experiment only the thione form was present, as ascertained by X-ray photoelectron spectroscopy.[9]

III. Computational Details

The static exchange (STEX) method used in the present calculations of the NEXAFS spectra is a separate state approach in which the excited state is approximated by the coupling of a target ionic state and an excited orbital optimized in the static field of the molecular ion. Its direct implantation has been extensively described elsewhere[2] and applied to different types of core electronic spectra.[3] In the STEX approach each excitation/ionization channel is considered separately and gives origin to a one-electron Hamiltonian containing a site specific $(N - 1)$-electron core potential. Such potential for the excited electron is static with respect to the ion−electron interaction, but the exchange interaction as well as the relaxation of the ion orbitals are fully accounted for.[2] The ionic reference state, as well as the ground state, are calculated at the Hartree−Fock level by projection on a standard Gaussian basis set that is then extended by additional diffuse functions centered at the ionized site (so-called double basis set technique) for the calculation of the STEX Hamiltonian matrix directly from one- and two-electron integrals. In the present calculations we adopted a Dunning basis set for C and N[10] (triple-ζ) and for H[10] (double-ζ plus polarizing). Sulfur requires a good d-function basis set to account for its coordination in the ground and excited states; a triple-d basis set is used in that case. For the calculation of the STEX Hamiltonian, augmentation of the basis sets with a large set of diffuse functions (20s, 18p, 20d) centered on the ionized site, has been employed. The geometry of MBT has been computed by SCF (self-consistent-field) optimization. Our previous investigation on a similar molecule, 2-mercapto-benzoxazole (MBO), has shown that small geometry variations produce negligible changes in the NEXAFS spectra. The integrated photoabsorption cross section is obtained by Stieltjes Imaging (SI)[11] on the discrete spectrum computed with the excitation levels converging to the specific channel ionization threshold that is determined by the ΔSCF procedure. STEX calculations at the C K-edge and S L-edge have been performed separately for each one of the inequivalent atoms. The computed spectra are finally convoluted with a Gaussian function of different full width at half-maximum (fwhm) for the three (C, N, S) edges (exact values are given in the text) in order to account for the experimental resolution and the vibrational broadening that is not considered in the present calculations under the vertical transition approximation. The major limitations of the STEX approximation are related to electron correlation effects and the effect of screening of the excited electron. While the former could be reduced to the relatively small correlation between the target and the excited electron, the residual relaxation of the bound electron due to the screening can be relevant for the lowest excited states of valence character. The missing screening results in energy errors that for core excitations to π^* orbitals are of about 1−2 eV.

IV. Results and Discussion

This section describes the experimental NEXAFS spectra of MBT and their interpretation with the support of the ab initio calculations. A comparison with the analogous spectra of 2-mercaptobenzoxazole (C_7H_5ONS, in the following MBO), a similar molecule with an oxygen atom instead of the sulfur in the pentatomic ring, which has been investigated previously,[12−14] is presented in the last subsection.

C and N K-edges and S L-edge spectra will be discussed separately in the following subsections.

A. Carbon K-Edge. The experimental total-ion-yield C K-edge spectrum recorded for MBT in the gas phase is reported in Figure 2; the low-energy region is also shown, with higher resolution, in the upper part of the figure. This spectrum shows four structured bands ("a" to "d") between 285 and 290 eV (clearly identifiable at 285.5, 286.2, 287.3, and 289.1 eV) and comparatively weaker and larger structures at higher energy (found at 295.5 and 300.7 eV).

Figure 3 collects the C K-edge spectra computed by the STEX method and convoluted with a Gaussian function (fwhm = 0.40 eV), for the seven inequivalent carbon atoms of MBT (from C_1 to C_7 in Figure 1) and the sum of these spectra (C_{tot}). The arrows mark the opening of the different ionization channels. Table 1 reports the main theoretical excitations (energy and oscillator strength) and the ΔSCF ionization thresholds for the seven channels. The total C K-edge (C_{tot}) spectrum, also reported in Figure 4, can be compared with the experimental one reported in Figure 2; a more detailed comparison of the main spectral features can be made for the low-energy region considering the experimental spectrum at higher resolution reported in the upper part of Figure 2.

From the STEX simulations in Figures 3 and 4 the first three transitions appearing in the low-energy region of the experimental spectrum, labeled from "a" to "c" in Figure 2, can be assigned to π^* resonances due to the chemically inequivalent carbon atoms. Carbon atoms C_2, C_3, C_4, and C_5 give rise to resonances close to each other and contributing to feature "a". The C_1 carbon atom gives rise to the resonance "b", while C_6 and C_7 atoms produce resonance "c". The fourth transition appearing in the experimental spectrum, labeled as "d" in Figure 2, can be assigned to a σ resonance due to the carbon atom C_1 and mainly localized on the C_1-S_1 bond.

Except for the energy shift due to the missing screening (as discussed in the Computational section) we find good agreement

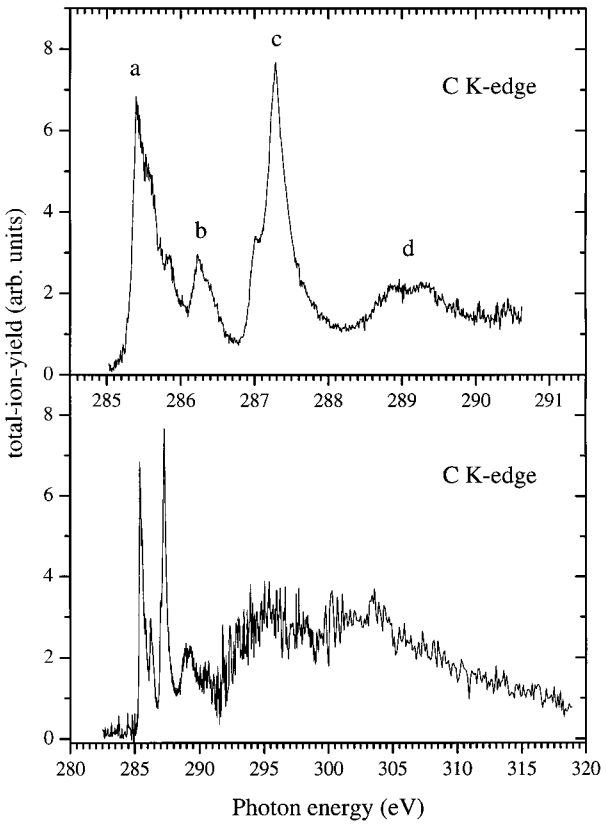

Figure 2. Experimental total-ion-yield C K-edge spectrum of gas-phase MBT. The high-resolution low-energy region is reported in the upper part.

between the main features of the experimental and calculated spectra. Beyond 291 eV multiple structures are observed due to onsets of the ionization edges. In MBT they extend over a large interval owing to the presence of several chemically different carbon atoms (see Tables 1 and 2). Discrete minor transitions in addition to the previously discussed resonances are predicted but are comparatively weak and not significant for the analysis.

The high-resolution spectrum in Figure 2 shows clearly that the main four bands "a" to "d" present structured shape due to a number of not fully resolved peaks. Their estimated energy position is reported in Table 2. Because the calculations have been performed in the vertical transition approximation, i.e., at fixed positions of the nuclei, such transitions could be tentatively ascribed to vibrational excitations. The differences in the intensity ratio of the four main spectral structures between experiment (Figure 2) and theory (Figure 4) can also be ascribed to neglecting of the nuclear motion in the theoretical model. This hypothesis is strongly supported by recent calculations[13] of the core excitation of MBO at the C K-edge, where vibrational effects have been explicitly included. The fine structure observed experimentally for MBO (and quite similar to that of MBT in Figure 2) could be firmly interpreted as due to vibrational excitations. It should be noted that the peak at 287.28 eV in Figure 2 is significantly narrower than the other peaks, then different vibrational contributions can be hypothesized for this transition with respect to the others. This peak can be ascribed to the C_7 atom by comparison with the MBO case, where the peak attributed to the C_7 atom, which is well separated in energy, presents a narrower fwhm in both experimental and calculated spectra due to different vibrational progression. Consequently, the structure at 287.02 eV can be

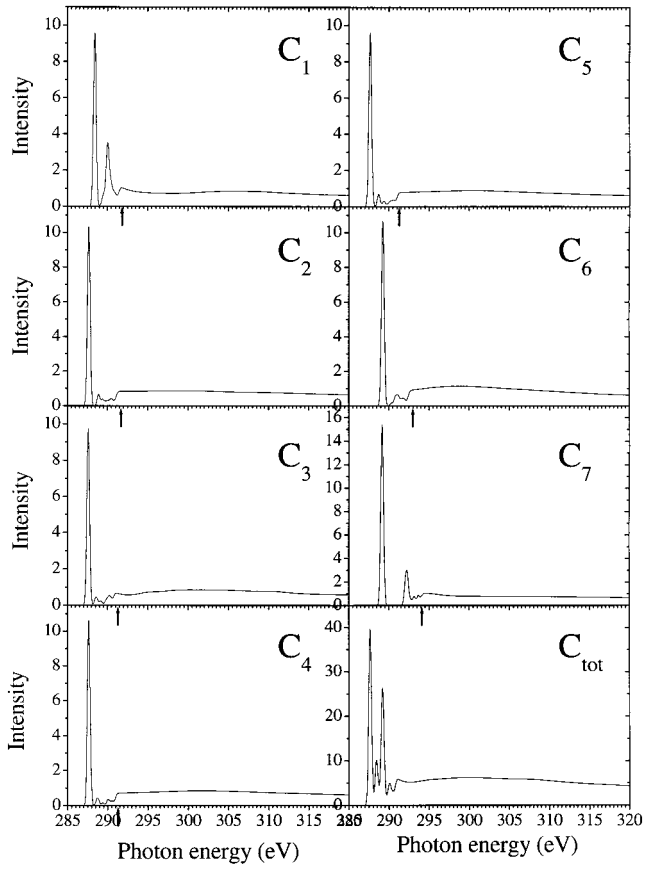

Figure 3. C K-edge spectra calculated by the STEX method for the seveninequivalent carbon atoms (C_1 to C_7) of MBT convoluted in the low-energy region with 0.40 eV fwhm Gaussian functions. The sum of the C_1 to C_7 K-edges spectra is indicated as C_{tot}. The absorption cross section (full line) is given in Mb; the absolute values of the oscillator strengths (bars) are reported in Table 1. Arrows mark the positions of the core ionization thresholds.

attributed to C_6. Calculations on MBT including explicitly vibrational effects will be the subject of a forthcoming investigation.

B. Nitrogen K-Edge. The experimental total-ion-yield N K-edge spectrum recorded for MBT in the gas phase is reported in Figure 5. The contribution to the N K-edge spectrum of N_2 present in the residual gas of the experimental chamber has been subtracted from the experimental spectrum using the pure N_2 spectrum recorded in the same experimental conditions. By changing the oven temperature, and therefore the MBT vapor pressure, we have recorded spectra with different relative MBT/N_2 concentrations. Those spectra were used to identify the features due to the N_2 molecule and to verify the correctness of the subtraction procedure. The π^* resonance of N_2 was vibrationally resolved and the first component at 400.88 eV does not overlap the lower energy band of MBT, so this feature provided an accurate guide to subtract the N_2 contribution from the MBT spectrum. In fact, a $\pm 5\%$ change in the relative intensity of the N_2 contribution subtracted from the spectrum gave a positive (or negative) "spurious peak" close to the onset of the first band of MBT. In the MBT spectrum two main peaks are evident at 401.4 and 402.9 eV, respectively, and a broad resonance is visible at 409 eV (see Table 2).

Figure 6 reports the computed spectrum at the N K-edge convoluted with 0.60 eV fwhm Gaussian function. In the upper part of the figure, the low-energy region is highlighted together with the bar diagram describing the energy position and intensity

TABLE 1: Main STEX Excitation Energies (below the Ionization Thresholds) and Oscillator Strengths (in Parentheses) at the C and N K-Edges and S L-Edge of MBT[a]

C K-edge	N K-edge	S L-edge
C_1	403.53 (0.0147) (π^*)	S1
288.42 (0.0372) (π^*)	404.31 (0.0046) (σ)	lower series ($2p_{3/2}$)
289.47 (0.0020) (σ)	405.53 (0.0059) (π)	166.93 (0.00436) (π)
289.85 (0.0043) (σ)	407.03 IP	167.18 (0.01063) (σ)
290.08 (0.0099) (σ)		167.44 (0.01451) (σ)
290.43 (0.0037) (σ)		169.28 (0.00315) (σ)
291.68 (0.0029) (σ)		169.65 (0.00307) (σ)
291.85 IP		169.77 (0.00225) (σ)
C_2		170.20 IP
287.66 (0.0402) (π^*)		upper series ($2p_{1/2}$)
288.89 (0.0026) (σ)		168.13 (0.00218) (π)
291.45 IP		168.38 (0.00531) (σ)
C_3		168.64 (0.00726) (σ)
287.59 (0.0378) (π^*)		171.40 IP
291.13 IP		S2
C_4		lower series ($2p_{3/2}$)
287.65 (0.0413) (π^*)		163.89 (0.00961) (π)
288.68 (0.0012) (σ)		166.09 (0.00285) (σ)
291.33 IP		167.23 (0.00242) (σ)
C_5		167.40 IP
287.67 (0.0373) (π^*)		upper series ($2_{1/2}$)
288.71 (0.0027) (σ)		165.09 (0.00481) (π)
291.38 IP		168.60 IP
C_6		
289.24 (0.0414) (π^*)		
290.82 (0.0021) (π)		
292.81 IP		
C_7		
289.16 (0.0599) (π^*)		
292.05 (0.0059) (σ)		
292.29 (0.0088) (σ)		
294.34 (0.0041) (σ)		
294.38 IP		

[a] For the C K-edge, the seven channels (C_1 to C_7) due to the seven inequivalent carbon atoms are included. For the S L-edge the two channels, due to the $2p_{3/2}$ and $2p_{1/2}$ core levels, for the two atoms (S_1 and S_2) due to the two inequivalent sulfur atoms are included. ΔSCF ionization thresholds (IP) are reported.

of the transitions (also reported in Table 1). The arrow in the figure shows the ionization threshold.

In the low-energy region the calculations predict three main discrete transitions at 403.53, 404.31, and 405.53 eV (with oscillator strengths 0.0147, 0.0046, and 0.0059, respectively). The first and third bands are due to excitations to out-of-plane orbitals (both fairly compact), while the second one involves a σ orbital localized along the N−H bond. The two transitions at 403.53 and 405.53 eV are mainly localized on N−C_7 and N−C_6 bonds, respectively. Comparison between calculated and experimental spectra shows good qualitative agreement, except for the expected energy shift of the theoretical excitations and the intensity ratio of the two main peaks. This intensity difference could be due to a larger core−hole overscreening effect (shift to higher energy of the excitation) for the lowest, more localized π excited state, with respect to the second one. A correction of the overscreening effect would lead to a σ transition relatively closer to the second π peak and to a theoretical intensity ratio of the two main peaks more similar to the experimental one. The higher photon energy resolution in the gas-phase experiment does not reveal additional fine structures because of the large intrinsic bandwidth of the transitions involved.

C. Sulfur L-Edge. The experimental total-ion-yield S L-edge spectrum recorded for MBT in the gas phase is reported in Figure 7. In the low-energy region, highlighted in the upper part of the figure, narrow resonances at 160.64, 161.75, 163.33, 164.59, 165.31, and 166.35 eV are observed, while broad resonances are visible at 172.0 and 180.6 eV (see Table 2). The S L-edge experimental spectrum of MBT powder reported in ref 4 presents the same main structures of the spectrum here reported. In our case, however, the higher photon energy resolution and the different nature of the sample (gas phase) permits the study of the fine structure.

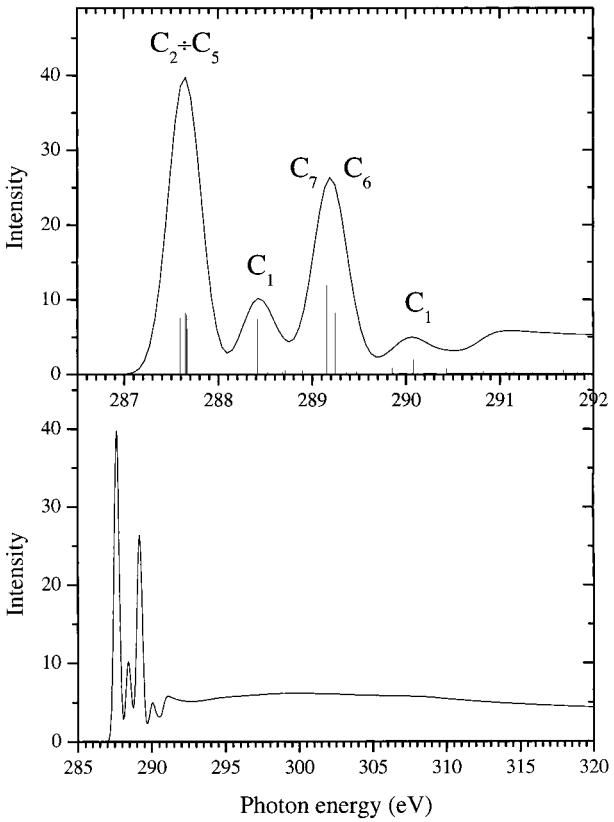

Figure 4. C K-edge spectrum calculated by the STEX method for MBT convolutedin the low-energy region with 0.40 eV fwhm Gaussian functions. In the upper part, the low-energy region is highlighted together with the bar diagram showing the energy position and intensity of the transitions and the attribution to the seven C atoms. The absorption cross section (full line) is given in Mb; the absolute values of the oscillator strengths (bars) are reported in Table 1.

TABLE 2: NEXAFS Experimental Energy Positions in the C and N K-Edges and S L-Edge Spectra of Gas-Phase MBT[a]

C K-edge	N K-edge	S L-edge
285.43 (0)	401.4 (0)	160.64 (0)
285.58 (0.15)	402.9 (1.5)	161.75 (1.11)
285.86 (0.43)	409 (7.6)	163.33 (2.69)
286.24 (0.81)		164.59 (3.95)
287.02 (1.59)		165.31 (4.67)
287.28 (1.85)		166.35 (5.71)
288.89 (3.46)		172.0 (11.36)
289.31 (3.88)		180.6 (19.96)
295.5 (10.07)		167.54 $2p_{3/2}$ IP
300.7 (15.27)		168.75 $2p_{1/2}$ IP
290.51 IP		169.97 $2p_{3/2}$ IP
290.63 IP		171.21 $2p_{1/2}$ IP
290.64 IP		
290.94 IP		
291.22 IP		
291.93 IP		
292.93 IP		

[a] The excitation energy relative to the lowest transition is shown in parentheses. Ionization thresholds (IP) from X-ray photoelectron spectra are reported for C 1s and S 2p levels.[9]

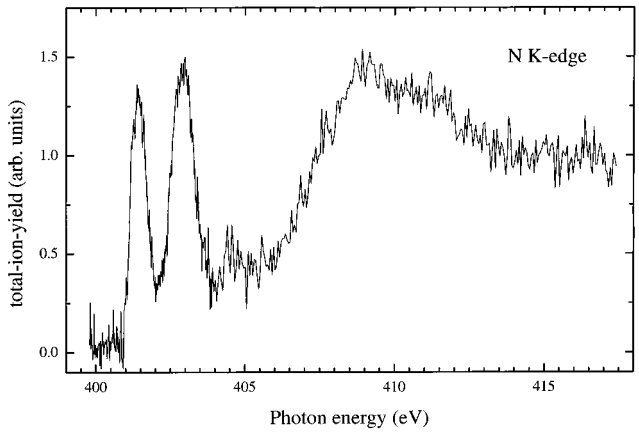

Figure 5. Experimental total-ion-yield N K-edge spectrum of gas-phase MBT.

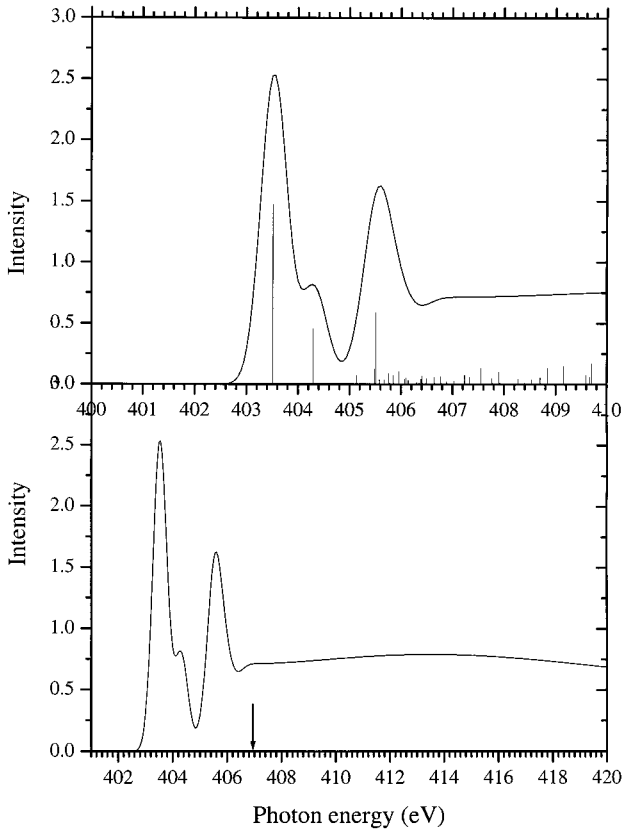

Figure 6. Calculated N K-edge spectra by the STEX method for MBT convoluted in the low-energy region with 0.60 eV fwhm Gaussian functions. In the upper part the low-energy region is highlighted together with the bar diagram describing the energy position and intensity of the transitions. The absorption cross section (full line) is given in Mb; the absolute values of the oscillator strengths (bars) are reported in Table 1. The arrow marks the position of the core ionization threshold.

The MBT S L-edge spectra computed for the two inequivalent sulfur atoms (endocyclic S_1 and exocyclic S_2, see Figure 1) convoluted with 0.40 eV fwhm Gaussian function, are reported in Figure 8. The sum of the S_1 and S_2 S L-edge spectra is indicated as S_{tot}. In the right part of the figure the low-energy region is highlighted together with the bar diagram describing the energy position and intensity of the transitions. The energy positions and the corresponding absolute values of the oscillator strengths (bars) for the calculated transitions are reported in Table 1. The arrows show the position of the core ionization thresholds for the S $2p_{3/2}$ (lower) and the S $2p_{1/2}$ (upper) channels for S_1 and S_2.

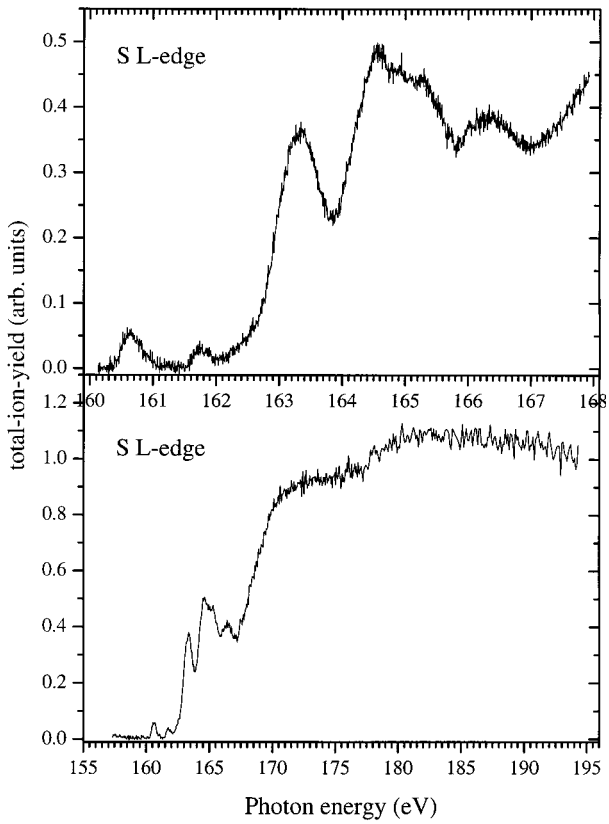

Figure 7. Experimental total-ion-yield S L-edge spectra of gas-phase MBT. The high-resolution low-energy region of the spectrum is reported in the upper part.

It should be considered that, apart for the presence of two inequivalent S atoms, the theoretical analysis of the S L-edge spectrum is complicated by the effect of the spin−orbit splitting that produces a duplication of the spectra and by the molecular field that splits the 2p atomic levels into quasi-degenerate sublevels with special implications for the static exchange analysis. The presence of the spin−orbit splitting is accounted for in a pragmatic way by superimposing two spectra shifted by the energy difference observed experimentally for the ionic states, assuming a statistical intensity ratio (2:1). Molecular field splitting of the 2p level implicates the appearance of "new" fine structure levels in high-resolution NEXAFS spectra of small species.[15] This effect is taken into account in the present molecular ΔSCF and STEX calculations. It leads to a splitting that is very small (0.07 eV for S_1 and 0.12 eV for S_2) if compared with the effective energy resolution in the experimental spectra. We therefore treat the excitation spectra for the different molecular "2p" subchannels as converging to a same (average) ionization threshold. Of more serious concern for the STEX analysis of MBT spectrum is the neglect of the channel coupling for excitations from quasi-degenerate molecular orbitals corresponding to the 2p level. The STEX approximation is in fact mainly designed for the representation of core excitations at the K-edge where the channels are decoupled because of energy or spatial separation of the core orbitals involved.

To take into account the experimental spin−orbit splitting value of 1.2 eV obtained from XPS spectra,[9,4] the $2p_{3/2}(L_3)$ channel spectrum has been obtained from the nonrelativistic results by subtracting $^1/_3$·1.2 eV from the calculated IP, while for the $2p_{1/2}(L_2)$ channel spectrum $^2/_3$·1.2 eV has been added. The corresponding oscillator strengths have instead been multiplied by their statistical weight factors, $^2/_3$ and $^1/_3$, respectively. The two (L_3, L_2) spectra for each inequivalent S

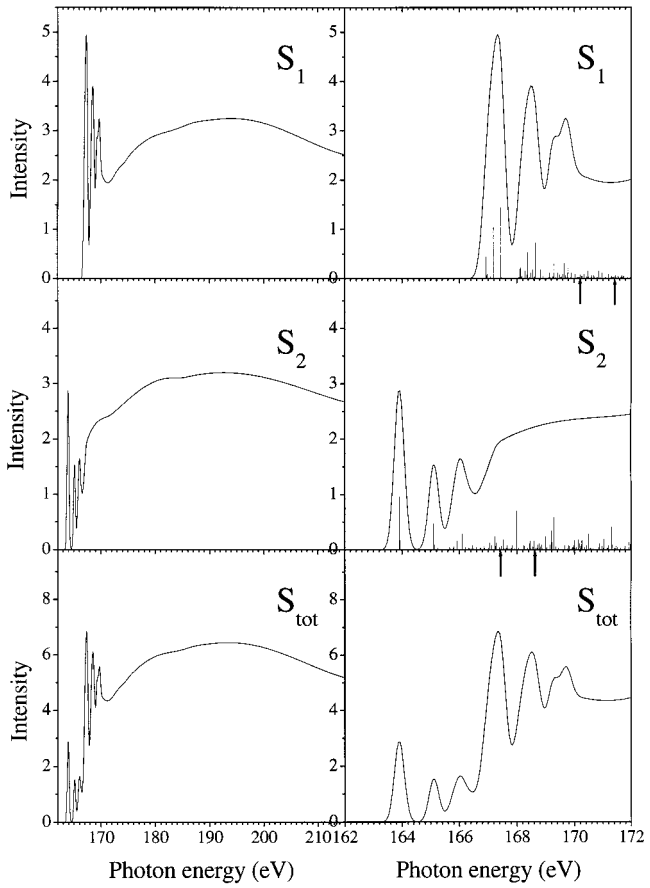

Figure 8. S L-edge spectra calculated by the STEX method for the two inequivalent sulfur atoms (S_1 and S_2) of MBT convoluted in the low-energy region with 0.40 eV fwhm Gaussian functions. The sum of the S_1 and S_2 S L-edge spectra is indicated as S_{tot}. In the right part, the low-energy region is enlarged together with the bar diagram describing the energy position and intensity of the transitions. The absorption cross section (full line) is given in Mb; the absolute values of the oscillator strengths (bars) are reported in Table 1. Arrows mark the positions of the core ionization thresholds.

atom were then added to give the S_1 and S_2 spectra reported in Figure 8. Their sum S_{tot} is the theoretical simulation of the total spectrum at the S L-edge, to be compared with the experimental one in Figure 7.

The experimental spectrum shows a low ratio of discrete to continuum intensity with basically six main resonance peaks followed by weaker Rydberg and multielectron excitations superimposed on a shape resonance structure close to the continuum. The first two peaks at 160.64 and 161.75 eV, which are clearly reproduced also in the calculated S_{tot} spectrum, are due to π excitations from the exocyclic S_2 atom, respectively, the $2p_{3/2}$ and $2p_{1/2}$ spin−orbit components. It should be noted that in the spectrum of the MBT powder[4] the second transition is partially overlapping with the next transition. The same difference was observed in the spectra of solid and gas-phase MBO[12,14] and ascribed to a shift of the π resonance due to intermolecular interactions in the solid state that modify the energy levels of the molecular orbitals involved in the transition.

In the higher energy region, the main difference between experiment and theory is the fact that the band predicted for the computed S_2 spectrum at 166.1 eV is not observed in the experimental spectrum as a resolved peak. This discrepancy could be ascribed to an overestimation of the energy difference between the computed 2p IPs for S_1 and S_2 atoms (2.80 eV); the experimental value is 2.43 eV (see Table 2). Using this smaller IP difference before summing the S_1 and S_2 calculated spectra, the structure at 166.1 eV in the S_2 merges with the structure at 167.2 in the S_1 spectrum, giving a better overall agreement with the experimentally observed spectrum in that energy region. The remaining structures at higher energy are due to a mixture of discrete excitations from S_1 and states in the continuum region of the S_2 (see Table 1).

TABLE 3: Comparison of the STEX Calculations Performed on the Carbon Atoms of MBT and MBO Molecules

	MBT C1s IP (eV)	π^* transition energy position (eV)	term value (eV)	MBO C1s IP (eV)	π^* transition energy position (eV)	term value (eV)
C_1	291.85	288.42	3.43	293.19	289.62	3.57
C_2	291.45	287.66	3.79	291.67	287.72	3.95
C_3	291.13	287.59	3.54	291.42	287.70	3.72
C_4	291.33	287.65	3.68	291.42	287.67	3.75
C_5	291.38	287.67	3.71	291.45	287.54	3.91
C_6	292.81	289.24	3.57	293.01	289.26	3.75
C_7	294.38	289.16	5.22	295.71	290.12	5.59

[a] C 1s Ionization potential (IP), first π^* transition energy position and term value in electronvolts for the seven carbons are reported.

The theoretical spectrum shows good overall agreement with the experimental except for some details of the structures below the threshold that are not perfectly reproduced. These minor differences can be reasonably ascribed to the approximations of the theoretical model, namely to the neglecting of the vibrational motion and of the channel coupling.

D. Discussion and Comparison with MBO. It is interesting to compare the experimental and theoretical spectra obtained for MBT with those obtained for the similar molecule MBO.[12,14] This comparison will highlight the change in the NEXAFS spectra due to the substitution of the oxygen atom, present in MBO, with a sulfur atom.

The strong feature at 285.5 eV in the C K-edge spectrum is observed in both MBO and MBT spectra and has been assigned to excitations localized at the C_2, C_3, C_4, and C_5 atoms, i.e., atoms of the benzene ring without substituents. This feature depends very little on the remaining molecular structure and serves as an excellent spectral fingerprint for the benzene ring.[16,17] The benzene carbons, unconnected to any substituent, give rise to π^* peaks that are gathered in a small energy interval, as has been also predicted for benzenes with strong substituents.[16,18]

The effect of the substitution of the oxygen atom with a less electronegative sulfur atom is observed in the IPs and the C 1s−π^* transitions of the carbon atoms in the heterocyclic ring. In MBO the oxygen atom is the most electronegative in the molecule (3.5 in Pauling's scale). It withdraws electron density mainly from the two nearest carbon atoms (C_1 and C_7), which have the highest IPs and π^* resonances at higher photon energy (see Table 3). As in MBT the most electronegative atom is the nitrogen (3.0), a rearrangement of the electron density in the heterocyclic ring is expected. The electron density on C_1 increases, and consequently, its IP becomes lower than the one of C_6. The corresponding resonance is shifted to lower energy. In the case of MBO, core excitation at the C_7 atom, connected to N, S, and O, produces a C 1s−π^* peak that is well separated in energy from the π^* transitions due to C_1 to C_6 atoms. This peculiarity has been used to study the adsorption of MBO on Pt(111).[19] Due to the different chemical environment of the C_7 atom in MBT, the corresponding C 1s−π^* transition is superimposed on the transition due to the C_6 atom. This leads

to a more intense structure in that region of the spectrum, with respect to MBO. It is also interesting to note that, in both MBT and MBO, the term value (difference between the IP threshold and the excitation energy) of the C 1s$-\pi^*$ transition at the C_7 atom is much larger than for the π^* excitations of the other channels (see Table 3). Although C_7 gives a well-separated peak in the carbon X-ray photoelectron spectrum of MBT (see Table 2[9]), their C 1s$-\pi^*$ transition overlaps in the absorption C K-edge spectrum the C 1s$-\pi^*$ transition of C_6. Despite of this overlap, the structure at 287.28 eV seems sharper in the MBT spectrum than in MBO. This is, in our opinion, an indication of a different vibrational envelope due to a different nuclear dynamics around this carbon atom.

As in the case of MBO, the nitrogen spectrum presents two π peaks in the discrete part. Despite that N is formally single bonded, it provides a large discrete-to-continuum intensity ratio similar to that observed, for instance, in pyridine.[20] One can perhaps explain this by a "residual" conjugated character and by the presence of the fused benzene ring.

The two N$-$C bond lengths found in MBT are 1.34 Å for the N$-C_7$ bond and 1.40 Å for the N$-C_6$ bond, similar to those found in MBO (1.34 Å and 1.41 Å for the N$-C_7$ and N$-C_6$ bonds, respectively). Those values are comparable to the nitrogen bond length in pyridine with a partial double bond, but considerably shorter than the typical length of a single N$-$C bond (1.48 Å). One accordingly finds a shape resonances quite far beyond the IP ($\simeq$7 eV).

A full comparison of MBT with MBO at the S L-edge is complicated by the fact that in MBT there are two chemically different sulfur atoms. In the lower photon energy range, where the excitations due to S_1 and S_2 in MBT are not overlapping, two peaks are observed for both molecules in the gas phase. This confirms the assignment of those S $2p_{3/2,1/2}-\pi$ transitions as originating from the exocyclic sulfur atom. ΔSCF calculations, both for MBT and MBO, estimate a molecular field splitting of the S L-shell IPs of about 0.10$-$0.20 eV. Those values are similar to the splitting measured in OCS,[21] but due to the much more complicated vibrational structure of the XPS and NEXAFS spectra of the molecules considered here, this effect is masked in the experimental spectra.

V. Conclusions

A full comparison between gas-phase experimental and ab initio calculated NEXAFS spectra of 2-mercaptobenzothiazole has been reported for the C K-, N K-, and S L-edges. The present results have been discussed in comparison with a previous study on a similar molecule, 2-mercaptobenzoxazole, and with a similar experimental investigation on MBT powder. The good general agreement between experiment and theory allowed a detailed discussion and attribution of the various features of the spectra. Vibrational contributions have been tentatively identified in the low-energy part of the C K-edge spectrum and will be the subject of a detailed analysis by a forthcoming computational simulation.

Acknowledgment. G.C. and V.DiC. acknowledge the financial support by "Istituto Nazionale di Fisica della Materia, I.N.F.M." for the measurements at the ELETTRA laboratory. G.C. thanks the Director of the "Istituto di Analisi dei Sistemi ed Informatica" (IASI, CNR) of Rome (Dr. G. Rinaldi) and the computer staff for the use of the computers to perform the calculations.

References and Notes

(1) Stöhr, J. *NEXAFS Spectroscopy*; Springer-Verlag, Berlin, 1992.
(2) Ågren, H.; Carravetta, V.; Vahtras, O.; Pettersson, L. *Chem. Phys. Lett.* **1994**, *222*, 75.
(3) Ågren, H.; Carravetta, V.; Vahtras, O.; Pettersson, L. *Theor. Chem. Acc.* **1997**, *97*, 14.
(4) Hallmeier, K.;Mayer, D.; Szargan, R. J. *Electron Spectrosc. Relat. Phenom.* **1998**, *96*, 245.
(5) Blyth, R. R.; Delaunay, R.; Zitnik, M.; Krempasky, J.; Krempaska, R.; Slezak, J.; Prince, K. C.; Richter, R.; Vondracek, M.; Camilloni, R.; Avaldi, L.; Coreno, M.; Stefani, G.; Furlani, C.; de Simone, M.; Stranges, S.; Adam, M. Y. *J. Electron Spectrosc. Relat. Phenom.* **1999**, 101$-$103, 959.
(6) Domke, M.; Mandel, T.; Puschmann, A.; Xue, C.; Shirley, D.; Kaindl, G.; Petersen, H.; Kuske, P. *Rev. Sci. Instrum.* **1992**, *63*, 80.
(7) Sodhi, R.; Brion, C. J. *Electron Spectrosc. Relat. Phenom.* **1984**, *34*, 363.
(8) Hudson, E.; Shirley, V.: Domke, M.;Remmers, G.; Puschmann, A.; Mandel, T.; Xue, C. *Phys. Rev. A* **1993**, *47*, 361.
(9) Contini, G.; Di Castro, V.; Stranges, S.; Richter, R.; Alagia, M. To be published.
(10) Dunning,T., Jr. *J. Chem. Phys.* **1971**, *55*, 716.
(11) Langhoff, P.W. In *Theory and Application of Moment Methods in Many-Fermion Systems*; Dalton, B., Grimes, S., Vary, J., Williams, S., Eds.; Plenum: New York, 1980; p 191.
(12) Carravetta, V.; Contini, G.; Plashkevych, O.; Ågren, H.; Polzonetti, G. J. *Phys. Chem. A* **1999**, *103*, 4641.
(13) Plashkevych, O.; Ågren, H.; Carravetta, V.; Contini, G.; Polzonetti, G. *Chem. Phys. Lett.* **2000**, *327*, 7.
(14) Contini, G.; Di Castro, V.; Stranges, S.; Richter, R.; Alagia, M. *J. Phys. Chem. A* **2000**, *104*, 9675.
(15) Magnuson, M.; Guo, J.; Såthe, C.; Glans, P.; Rubensson, J.; Nordgren, J.; Yang, L.; Sałek, P.; Ågren, H. *Phys. Rev. A* **1999**, *59*, 4281.
(16) Pettersson, L.; Ågren, H.; Schürmann, L. B.; Lippitz, A.; Unger, W. *Int. J. Quantum Chem.* **1997**, *63*, 749.
(17) Carravetta, V.; Polzonetti, G.; Iucci, G.; Russo, M.; Paolucci, G.; Barnaba, M. *Chem. Phys. Lett.* **1998**, *288*, 37.
(18) Plachkevytch, O. ;Yang, L.; Vahtras, O.; Ågren, H.; Pettersson, L. *Chem. Phys.* **1997**, *222*, 125.
(19) Contini, G.; Carravetta, V.; Parent, P.; Laffon, C.; Polzonetti, G. *Surf. Sci.* **2000**, *457*, 109.
(20) Horsley, J.; Stöhr, J.; Hitchcock, A.; Newbury, D.; Johnson, A.; Sette, F. *J. Chem. Phys.* **1985**, *83*, 6099.
(21) Siggel, M.; Field, C.; Saethre, L.; Børve, K.; Thomas, T. J. *Chem. Phys.* **1996**, *105*, 9035.